Journal of the Serbian Society for Computational Mechanics / Vol. 18 / No. 2, 2024 / pp 110-127 / original paper
(10.24874/jsscm.2024.18.02.07)

FLOW AND HEAT TRANSFER OF NON-NEWTONIAN FLUIDS IN CONFINED TRIANGULAR GEOMETRIES: A COMPUTATIONAL APPROACH

Youcef Lakahal [0009-0005-7444-4880] **and Houssem Laidoudi*** [0000-0001-8700-7077]

University of Science and Technology of Oran Mohamed-Boudiaf USTOMB, Faculty of Mechanical Engineering, BP 1505, El -Menaouer, Oran 31000, Algeria
e-mail: houssem.laidoudi@univ-usto.dz, youcef.lakahal@univ-usto.dz
*c*orresponding author*

Abstract

This study examines mixed convection heat transfer in a lid-driven triangular cavity containing three heated horizontal finned cylinders immersed in power-law fluids. The cavity features inclined sidewalls maintained at a cold temperature, while the top adiabatic lid moves at a uniform velocity. The objective is to analyze the fluid's behavior and its influence on flow structure, heat transfer, and drag coefficients under varying conditions, including lid speed, thermal buoyancy intensity, and fluid viscosity characterized by the power-law index. The study employs numerical simulations based on the finite volume method to solve the governing equations, with the fluid's rheological behavior modeled using Ostwald's law. Results show that the heat transfer rate increases with Re, Ri, and n, with the bottom cylinder (C3) exhibiting the highest rate due to strong buoyancy and focused recirculation zones. The drag coefficient (C_D) decreases with Re but varies significantly with n, leading to higher drag forces for shear-thinning fluids. These findings provide new insights into optimizing heat transfer and drag in non-Newtonian fluid systems.

Keywords: mixed convection, complex fluid, numerical investigation, Nusselt number, drag coefficient, CFD

1. Introduction

Recent research has increasingly focused on the mixed heat transfer of rheologically complex fluids due to their wide-ranging applications in industries such as metallurgy, food processing, glass manufacturing, medical engineering, and oil exploration.

Several studies have investigated forced convection in non-Newtonian fluids, where the fluid flow is externally driven. For instance, Helmaoui et al. (2019), Mishra et al. (2017), and Mohebbi et al. (2019) explored flow and heat transfer properties of power-law fluids around confined cylinders with varying cross-sectional shapes, in an adiabatic square enclosure with single inlet and outlet ports, and between two parallel plates filled with partially porous media.

Other researchers have examined natural convection, where fluid motion arises due to buoyancy effects caused by temperature differences. Malkeson et al. (2023) and Rashid et al.

(2023) analyzed power-law fluid behavior in 2D trapezoidal enclosures with heated bottom walls, adiabatic top walls, and cooled inclined sidewalls, as well as in wavy cavities containing a fixed heated circular center with cold sidewalls. Lamsaadi et al. (2005, 2006) further investigated the effect of non-Newtonian behavior on convection onset, fluid flow, temperature fields, and heat transfer in shallow rectangular and vertical rectangular cavities with varying heating conditions.

Numerical studies have also explored mixed convection characteristics of power-law fluids in cavities. These works focus on the effects of key dimensionless parameters such as the Richardson number (Ri), Reynolds number (Re), and power-law index (n). Forced convection in such configurations is often driven by wall or lid motion, with some boundaries maintained at constant temperatures while others are thermally insulated (Mahmood et al. 2024; Bilal et al. 2022; Roy et al. 2023; Prasad et al. 2019; Thohura et al. 2021; Hussain et al. 2021). Mixed convection scenarios have also included cavities containing uniformly heated obstacles at their geometric centers (Çolak et al. 2021; Kumar et al. 2021; Gangawane and Oztop 2020a, 2020b; Vijayan and Gangawane 2020; Manchanda and Gangawane 2018; Gangawane and Gupta 2018; Gangawane et al. 2018).

Additionally, mixed convection heat transfer of non-Newtonian fluids with two inner rotating cylinders has been studied under varying thermal boundary conditions. Results, often presented as streamlines, isotherms, temperature profiles, and Nusselt numbers, demonstrate that the average Nusselt number is influenced by the rotational speed of the cylinders (Aboud et al. 2020; Khanafer et al. 2019; Barnoon et al. 2019; Selimefendigil and Öztop 2018; Garmroodi et al. 2019; Mokeddem and Laidoudi 2022). Other numerical simulations have examined mixed convection heat transfer in specialized geometries. For example, some studies have explored lid-driven triangular cavities filled with power-law nanofluids and subjected to inclined magnetic fields. Governing parameters, including Re, Ri, power-law index (n), and magnetic field angle, were analyzed, showing that the inclination angle can effectively control heat and mass transfer (Selimefendigil and Chamkha 2019; Hussain and Oztop 2021).

Non-Newtonian fluid flow through porous media has also attracted attention due to its importance in heat transfer and energy systems. Investigations have focused on the interaction between convection intensity, fluid rheology, and cavity porosity, aiming to identify optimal conditions for heat transfer (Rehman et al. 2024; Bilal et al. 2022; Kolsi et al. 2022). Experimental studies have assessed the role of baffles within square cavities, while 3D numerical simulations have examined mixed convection and entropy generation in cavities with central heated blocks (Rehman et al. 2024; Al-Rashed et al. 2018). Furthermore, laminar natural convection of power-law fluids in trapezoidal enclosures has been studied under varying Rayleigh numbers, power-law indices, and sidewall inclination angles (Malkeson et al. 2023). Mixed convection heat transfer in double lid-driven cubic cavities containing different heat sources has also been explored, showing significant effects of nanoparticle volume fraction, Ri, and Re on heat transfer and velocity profiles (Zhou et al. 2018).

Despite extensive research on mixed convection, the problem of three horizontal finned cylinders placed inside a lid-driven triangular cavity remains largely unexplored, despite its significant technological applications. This study aims to analyze the mixed convection of power-law fluids in the space between the triangular cavity walls and the three inner cylinders. Specifically, it presents new findings on the effects of Reynolds and Richardson numbers, as well as the fluid's rheological properties, on the flow and heat transfer characteristics. Furthermore, the overall drag coefficient and Nusselt number are calculated to clarify the influence of these parameters on the thermal and dynamic behavior of the system.

2. Physical problem and mathematical formulations

Figure 1 illustrates the computational domain used for this investigation. It comprises three horizontal finned cylinders positioned inside a lid-driven triangular cavity. The cylinders C1, C2 and C3 are maintained at a hot temperature T_h, while the left and right inclined sidewalls are kept at a cold temperature T_c ($T_h > T_c$). Additionally, the top adiabatic wall moves from left to right with a uniform velocity V0. The space between the cylinders and the triangular cavity is assumed to be filled with power law fluids. Three values of the power-law index (n) were considered (= 0.6, 1 and 1.6).

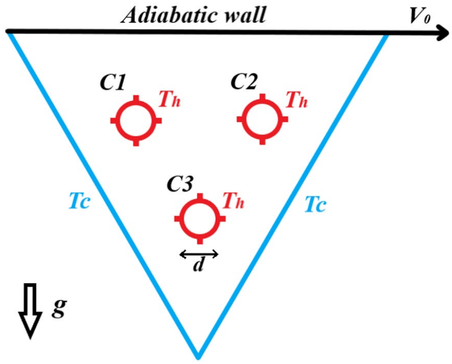

Fig. 1. Diagrammatic representation of the problem.

Mixed convection arises when both natural and forced convection mechanisms contribute to heat transfer. In this study, forced convection is induced by the motion of the adiabatic lid, while natural convection is driven by the temperature difference between the surfaces of the three cylinders and the inclined sidewalls. The Reynolds number determines the speed of the moving lid, while the Richardson number quantifies the balance between forced and natural convection effects. Four Richardson numbers are analyzed: 0, 1, 2, and 3.

The assumptions of laminar and non-Newtonian flow, steady state, mixed convection and constant fluid properties are adopted in this study. The equations of continuity, momentum, and energy subject to the Boussinesq approximation and the effect of negligible dissipation are written in their dimensionless form as follows:

The equation of continuity:

$$\frac{\partial u^*}{\partial x^*}+\frac{\partial v^*}{\partial y^*}=0 \tag{1}$$

The equation of momentum along the x-direction:

$$u^*\left(\frac{\partial u^*}{\partial x^*}\right)+v^*\left(\frac{\partial u^*}{\partial y^*}\right)=-\frac{\partial p^*}{\partial x^*}+\frac{1}{Re}\left(\frac{\partial \tau_{xx}^*}{\partial x^*}+\frac{\partial \tau_{yx}^*}{\partial y^*}\right) \tag{2}$$

The equation of momentum along the y-direction:

$$u^*\left(\frac{\partial v^*}{\partial x^*}\right)+v^*\left(\frac{\partial v^*}{\partial y^*}\right)=-\frac{\partial p^*}{\partial y^*}+\frac{1}{Re}\left(\frac{\partial \tau_{xy}^*}{\partial x^*}+\frac{\partial \tau_{yy}^*}{\partial y^*}\right)+Ri\times T^* \tag{3}$$

The equation of energy:

$$u^*\left(\frac{\partial T^*}{\partial x^*}\right)+v^*\left(\frac{\partial T^*}{\partial y^*}\right)=\frac{1}{Pe}\left(\frac{\partial^2 T^*}{\partial x^{*2}}+\frac{\partial^2 T^*}{\partial y^{*2}}\right) \tag{4}$$

Re and Pe are the Reynolds and Peclet numbers, Ri is the Richardson number, and u^* and v^* are the fluid dimensionless velocities in the x^* and y^* directions. Dimensionless pressure and temperature are represented by the numbers p^* and T^*, respectively. The following represents the dimensionless variables:

$$x^*=x/d\,,\ y^*=y/d\,,\ u^*=u/\left(V_0\right),\ and\ v^*=v/\left(V_0\right) \tag{5}$$

$$p^*=p/\rho\left(V_0\right)^2,\ T^*=(T-T_C)/(T_h-T_C) \tag{6}$$

$$Pe=\mathrm{Re}\times\mathrm{Pr} \tag{7}$$

The following equation represents the power-law fluid's behavior:

$$\tau_{ij}=2\eta\varepsilon_{ij} \tag{8}$$

where the viscous stress tensors and the rate of deformation are represented, respectively, by ε_{ij} and τ_{ij}. Furthermore, for power-law fluids, the fluid viscosity, denoted by η, is defined (in dimensional form) as follows:

$$\eta=m\left(\frac{I_2}{2}\right)^{\left(\frac{n-1}{2}\right)} \tag{9}$$

where I_2 is the second invariant of the rate of deformation tensor, m is the consistency index, and n is the power-law index. A fluid that is shear-thinning is represented by $n < 1$, a Newtonian limit by $n = 1$, and a shear-thickening fluid by $n > 1$. The following equation gives I_2 in Cartesian coordinates:

$$\left(\frac{I_2}{2}\right)=2\left(\frac{\partial u}{\partial x}\right)^2+2\left(\frac{\partial v}{\partial y}\right)^2+\left[\left(\frac{\partial u}{\partial y}\right)+\left(\frac{\partial v}{\partial x}\right)\right]^2 \tag{10}$$

Generally, Grashof number and Richardson number for power law fluids are computed as follows:

$$Gr=\left(g\beta_T\Delta T d^{(2n+1)}V_0^{(2-2n)}\right)/m^2 \tag{11}$$

$$Ri=\frac{g\beta_T\Delta T d\times V_0^{(n-2)}}{\left(\Omega\times d\right)^2}=\frac{Gr}{\mathrm{Re}^2} \tag{12}$$

where ρ, g, and β_T are the density of the fluid, the gravitational acceleration and volumetric expansion coefficient, respectively.

The drag coefficient is given by the following expression:

$$C_D=\frac{2F_D}{\rho V_0^2 d} \tag{13}$$

F_D is the total drag force on the surface of the cylinder.

The average Nusselt number, or Nu, is calculated by integrating local values along the inner cylinder's surface. The following are Nu's average and local values:

$$Nu_L = \left(\frac{\partial T^*}{\partial n}\right)_{wall} \quad , \quad Nu = \frac{1}{A}\int_s Nu_L dA \tag{14}$$

3. Numerical procedure

The present study was conducted using ANSYS-CFX, which transforms the governing equations of heat transfer and fluid mechanics into an algebraic system. The finite volume method was employed to solve these equations after applying the appropriate boundary conditions to the system's edges. The convergence criterion for the calculations was set to 10^{-6} for both the thermal transfer and fluid mechanics equations. A high-resolution scheme was used to discretize the convective terms, while the pressure-velocity coupling was solved using the SIMPLEC algorithm.

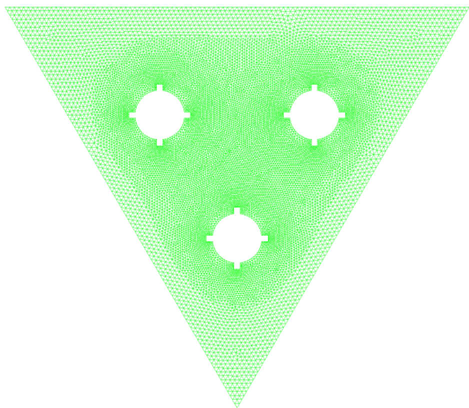

Fig. 2. The structure of the grid used for the calculations.

In the numerical simulation, the accuracy of the results is highly influenced by the number of grid elements, making the selection of an appropriate grid crucial (Fig. 2). To determine this, a grid independence test was performed. Table 1 summarizes the grid independence process, where three meshes of varying densities were generated. For each mesh, the Nusselt numbers (Nu) of the three cylinders Nn1, Nu2 and Nu3 were calculated under the conditions n=1.6, Re=15, and Ri=3. The results indicate that Mesh M2 is optimal, as it shows negligible differences in Nu values compared to the finer Mesh M3, while maintaining computational efficiency.

Mesh	Elements	Nu1	Nu2	Nu3
M1	125,000	1.73724	1.73993	3.21582
M2	250,000	1.76331	1.76604	3.26407
M3	500,000	1.76350	1.76623	3.26442

Table 1. Grid independency test for n = 1.6, Re = 15 and Ri = 3.

The validity of the numerical computational model was verified through comparisons with the results of two previous studies (Kuehn and Goldstein 1976; Matin and Khan 2013). The first comparison focused on buoyancy-driven flow between two concentric cylinders and evaluated the effect of the Rayleigh number (Ra = Pr · Gr) on the Nusselt number for Pr = 0.71 and n = 1, as shown in Fig. 3(A). The comparison demonstrated satisfactory agreement, confirming the model's accuracy. The second comparison investigated the influence of the non-Newtonian behavior of the fluid, specifically the effect of the power-law index (n), using data from Matin et al. (2013). The results, presented in Fig. 3(B) for Pr = 100 and a blockage ratio of 0.25, highlighted the variation of the Nusselt number with the power-law index. Once again, the numerical results aligned well with the reference data, validating the model's reliability.

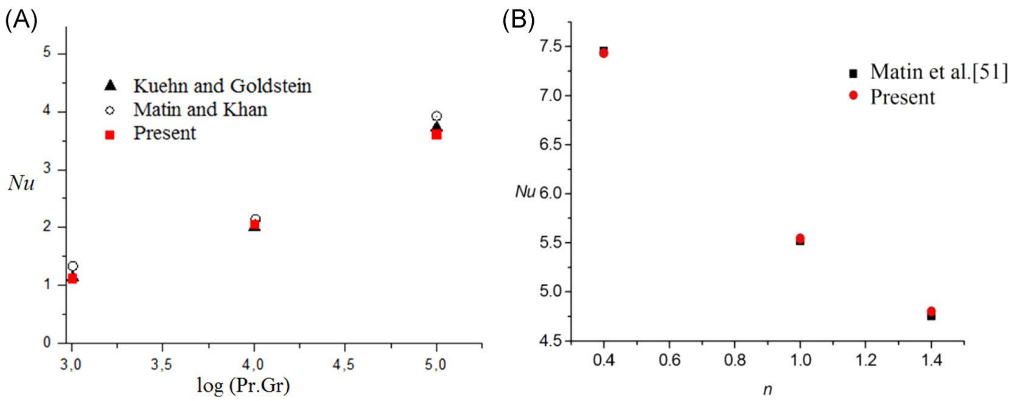

Fig. 3. The structure of the grid used for the calculations.

4. Results and discussion

This section provides a detailed presentation and discussion of the streamlines, isotherm contours, average Nusselt number and Drag coefficient for varying values of the power-law index (n), Reynolds number (Re), and Richardson number (Ri). The streamline and isotherm contours illustrate the fluid flow and thermal patterns, respectively. For the specified governing parameters of Ri (0, 1, 2, and 3), Re (5, 15, and 30), and n (0.6, 1.0, and 1.6) with a fixed Pr = 50, the Nusselt number (Nu) and Drag coefficient (CD) of the inner three cylinders (C1, C2, and C3) are determined. The selected parameter values are based on a previous study (Laidoudi and Ameur 2020).

Mixed convection occurs when both forced and natural convection take place simultaneously. In this study, natural convection is driven by the temperature difference between the inner finned cylinders and the left and right inclined sidewalls, while forced convection results from the moving lid.

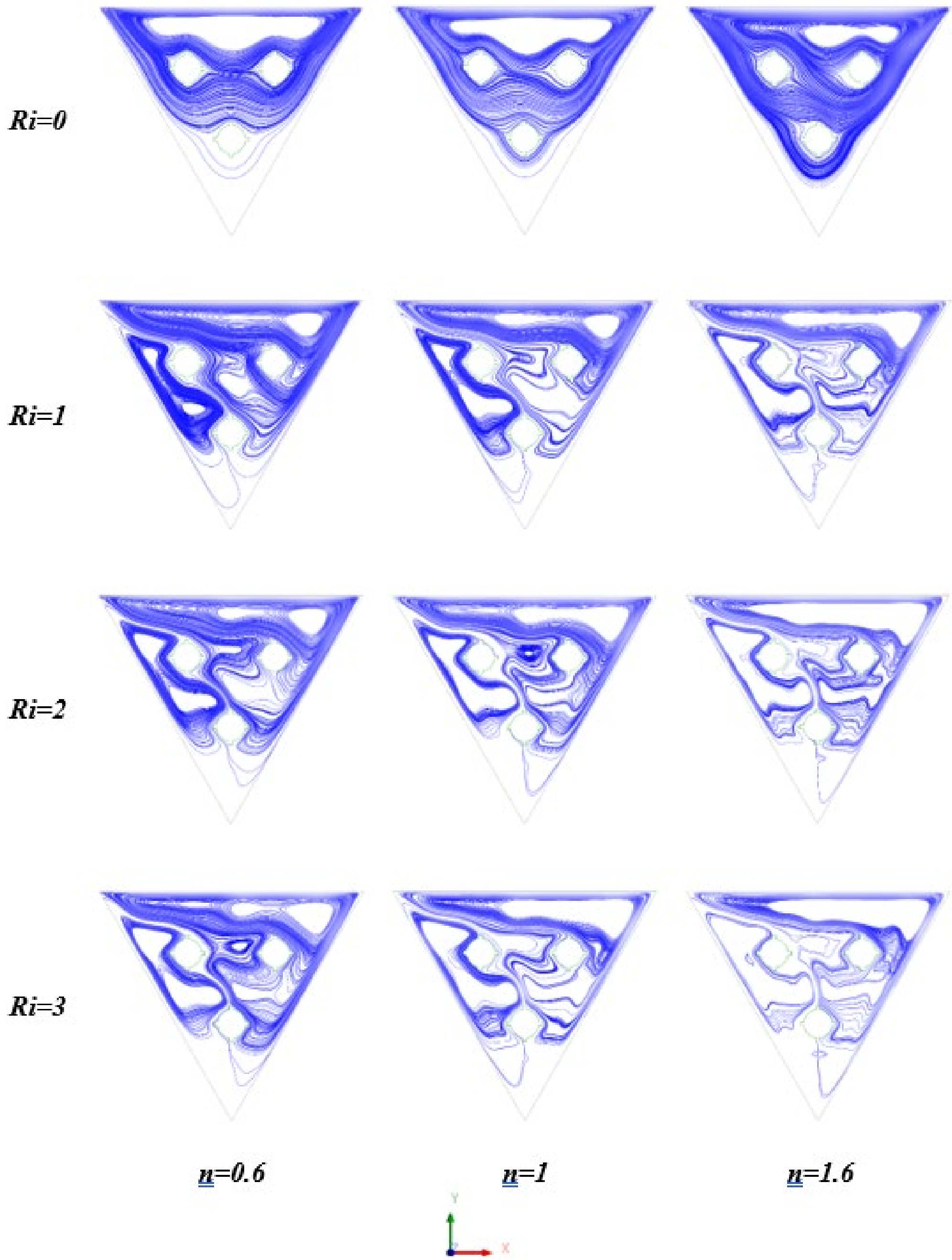

Fig. 4. Streamlines with various values of Ri and n at Re = 5.

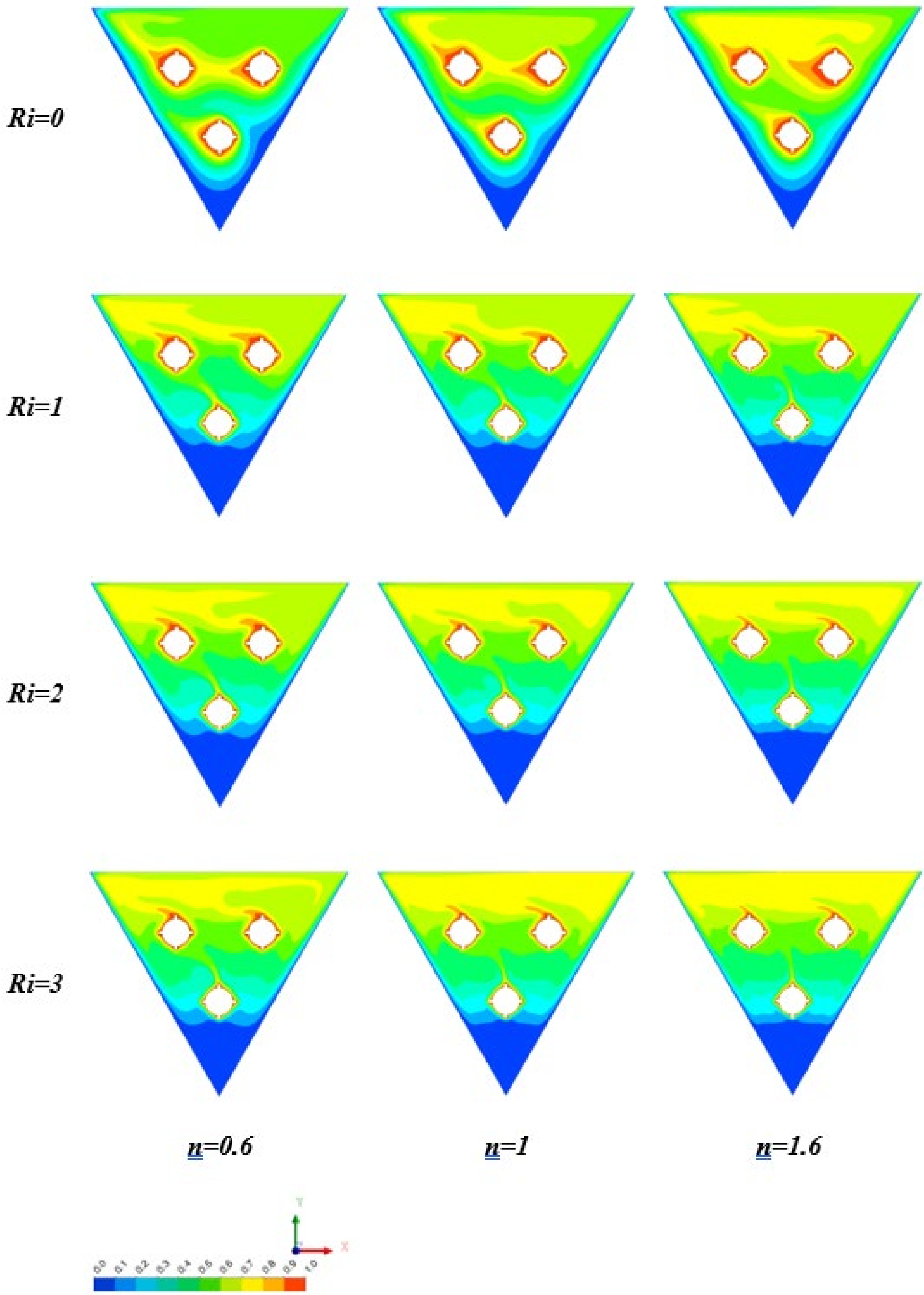

Fig. 5. Isotherms with various values of Ri and n at Re = 5.

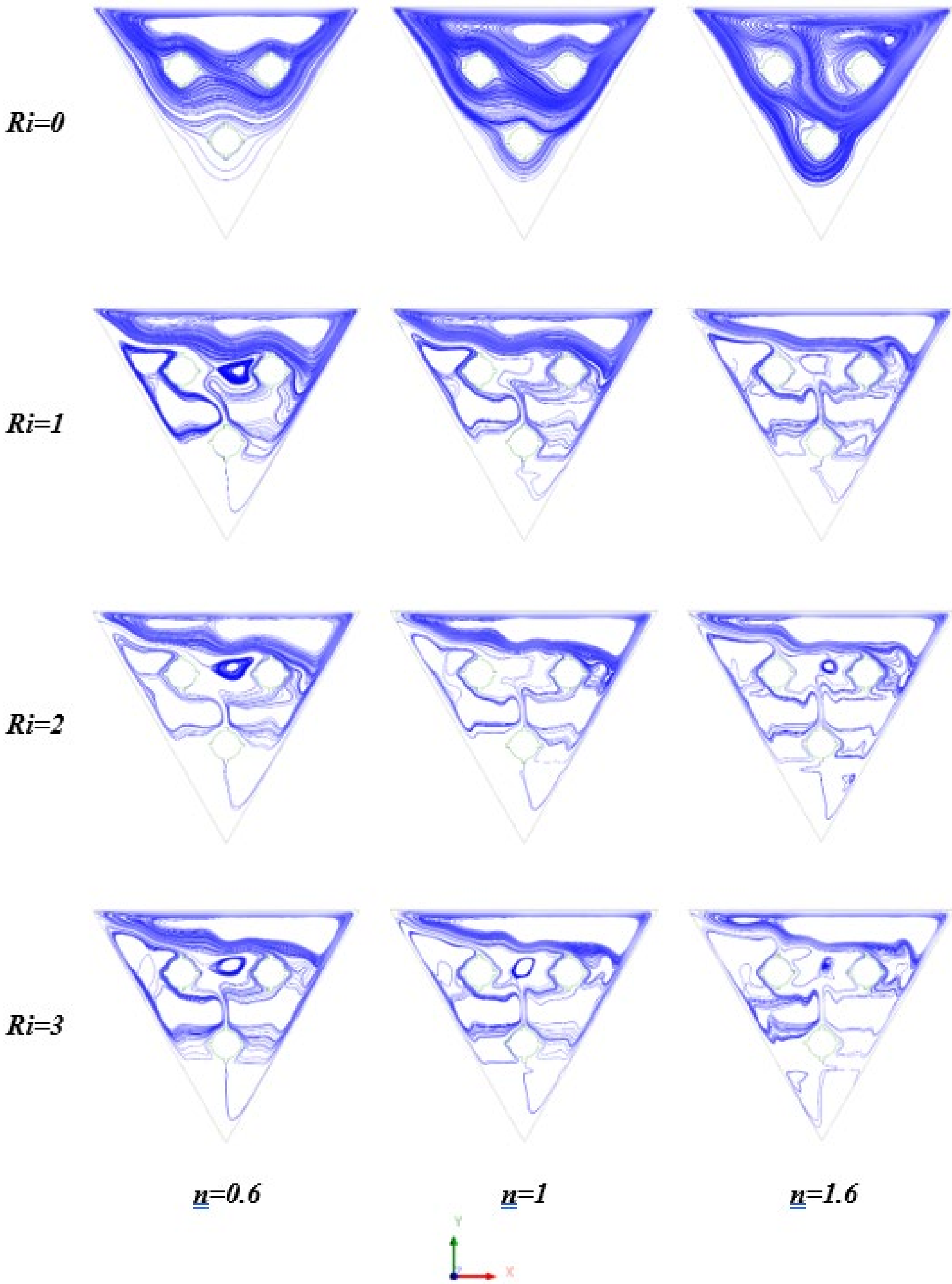

Fig. 6. Streamlines with various values of Ri and n at Re = 15.

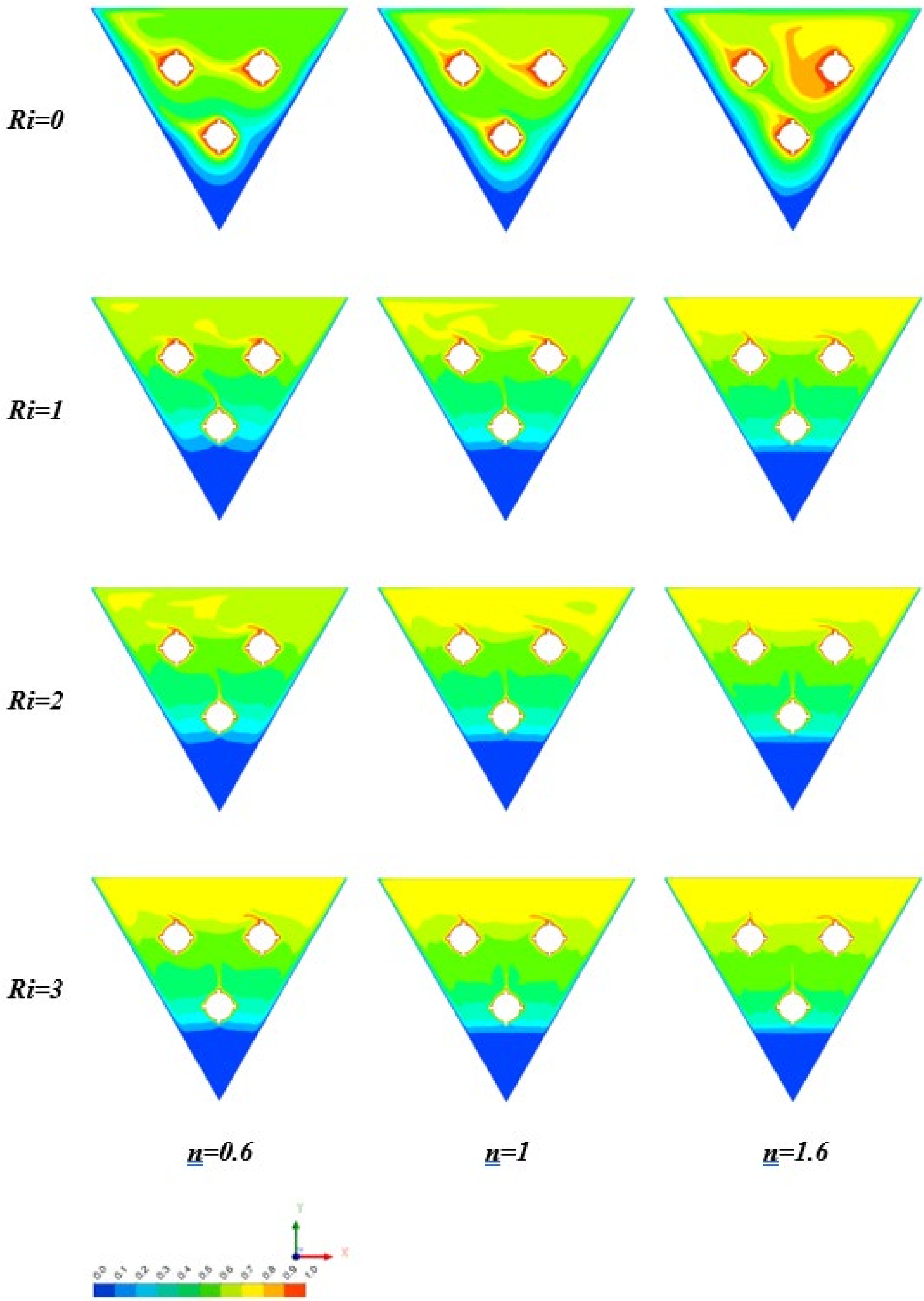

Fig. 7. Isotherms with various values of Ri and n at Re = 15.

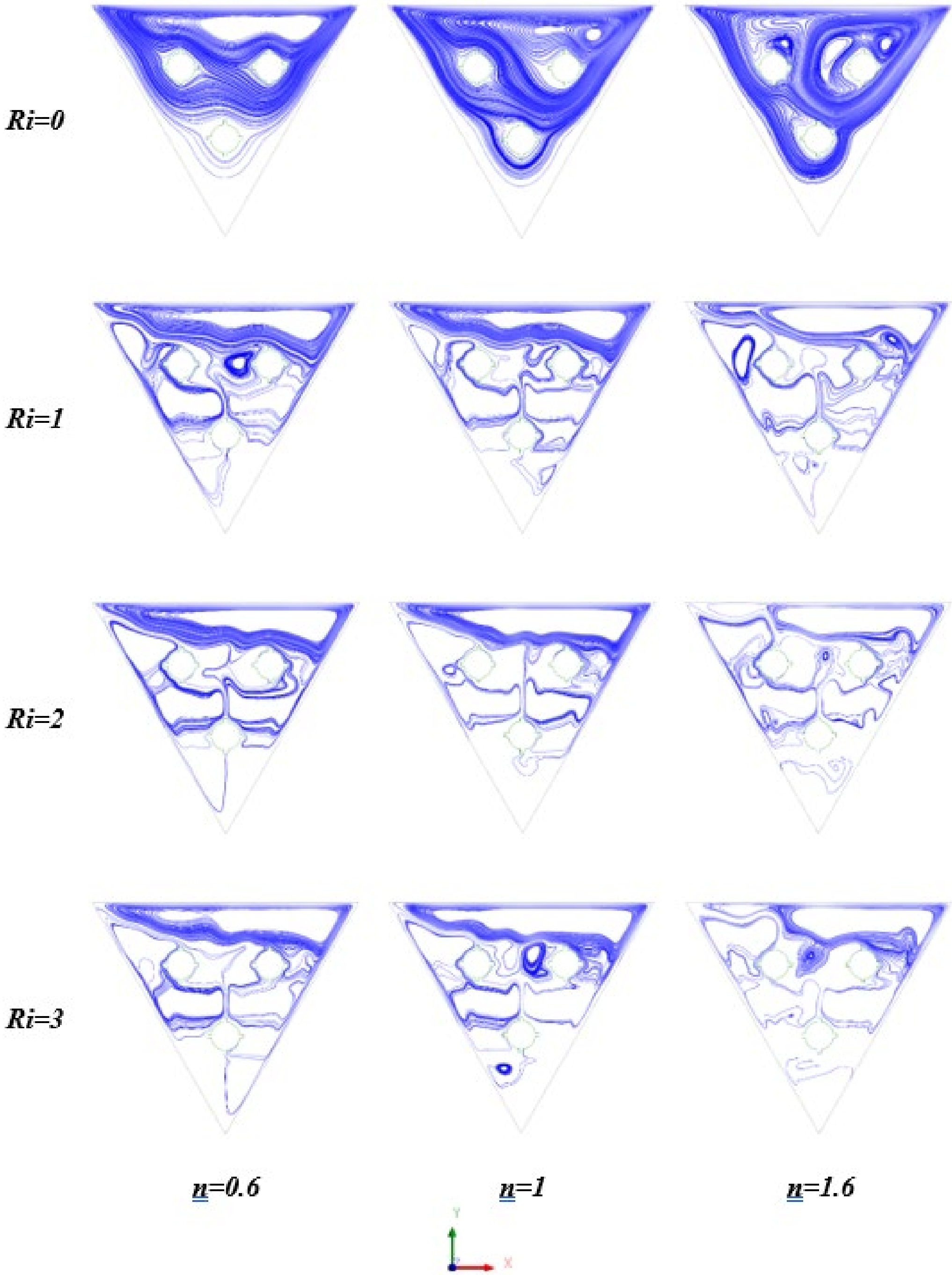

Fig. 8. Streamlines with various values of Ri and n at Re = 30.

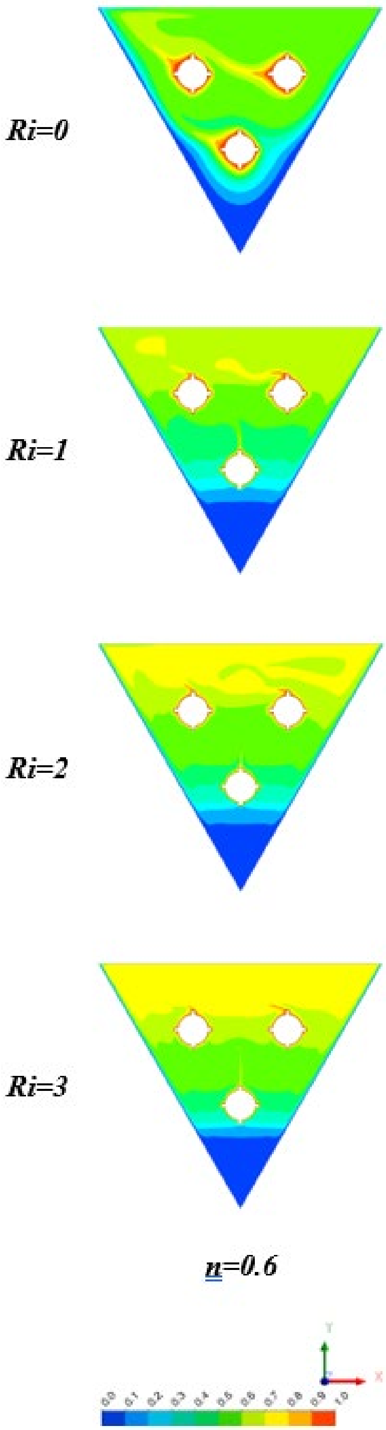

Fig. 9. Isotherms with various values of Ri and n at Re = 30.

When Ri = 0, only forced convection is dominant. As the Ri value increases, the buoyancy force, representing the effect of natural convection, also gradually increases. Meanwhile, the speed of the moving lid is directly related to the Reynolds number (Re).

The streamlines in the region between the triangular cavity and the finned cylinders are shown in Fig. 4. These streamlines provide a detailed visualization of particle trajectories and flow fields, helping to identify stagnant and counter-rotating regions. The effects of the Richardson number (Ri) and power-law index (n) on the streamlines at Re=5 are illustrated in Fig. 4. The flow exhibits steady rotation in the space between the cylinders and the triangular cavity, forming a vortex in the upper region. This vortex shifts toward the positive x-axis and diminishes in size as the power-law index increases (n = 0.6, 1, and 1.6) under pure forced convection (Ri = 0). In the mixed convection regime (Ri ≠ 0), a closed counter-rotating region with two loops appears on the left side of the space, while other forms in the upper region. As the values of Ri and n increase, the vortices merge and grow in size.

The streamlines for Re=15 and 30 are presented in Figs. 6 and 8. As the Richardson number (Ri), which represents the buoyancy force, and the Reynolds number (Re), indicative of lid velocity, increase, the vortex structures expand along both the x- and y-axes. Moreover, an increase in the power-law index (n) results in a reduction in the overall vortex size under conditions of pure forced convection. A distinct vortex is observed to the left of cylinder (C2) when n=1.6 at Re=30. For n=0.6, the fluid demonstrates shear-thinning behavior, where a decrease in dynamic viscosity with increasing shear stress facilitates particle movement. Conversely, for n=1.6, the fluid exhibits shear-thickening behavior, with dynamic viscosity increasing alongside shear stress, leading to enhanced flow stability. In the mixed convection regime, buoyancy forces predominantly influence the flow characteristics, playing a critical role in the formation of vortices.

The thermal fields in the region between the inner cylinders and the triangular cavity are depicted in Fig. 5, utilizing the same parameter values for n, Ri, and Re as in previous conditions. The thermal distribution closely follows the fluid flow pattern. On the right side of the cylinders, the movement of the lid enhances heat transfer. In contrast, fluid recirculation on the left side causes an increase in the thickness of the isotherms near the cylinders, indicating a reduction in the local temperature gradient. Overall, the dimensionless temperature gradient around the cylinders decreases with increasing n and Ri under mixed convection conditions (Ri≠0), but it increases as the power-law index n rises in the case of pure forced convection (Ri=0). Additionally, at higher Richardson numbers, the temperature distribution shifts toward the upper region of the triangular domain, indicating the dominance of buoyancy forces over the inertial forces generated by the lid. Consequently, the maximum temperatures are observed in the top portion of the cavity.

Figures 7 and 9 illustrate the thermal fields inside the triangular cavity at Re=15 and Re=30. The dimensionless temperature gradient around the cylinders generally decreases with increasing Re, except in the specific case of n=1.6 and Ri=0 at cylinder C2. In this case, the dimensionless temperature gradient increases with Re due to the expansion of the stagnant zone on the left side of cylinder C2, which inhibits heat transfer. Moreover, higher values of Re, Ri, and n contribute to enhanced convective heat transfer. The combined effects of buoyancy forces and lid movement promote efficient heat transfer to the top region of the cavity. As a result, the third cylinder (C3) experiences improved cooling performance.

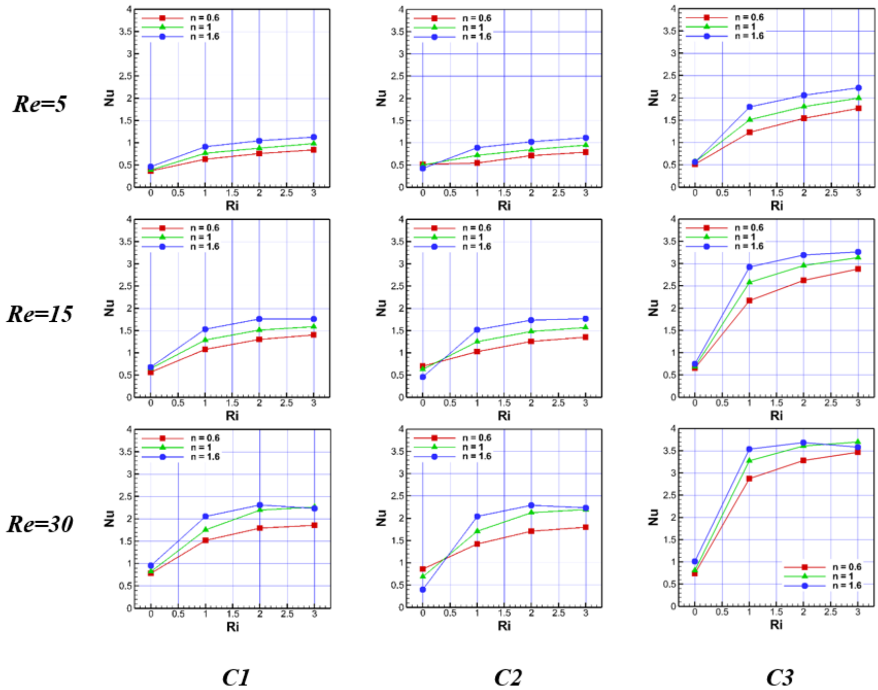

Fig. 10. Values of Nu versus Ri, n, and Re for each cylinder.

Figure 10 illustrates the variation of the Nusselt number (Nu) as a function of the Richardson number (Ri), power-law index (n), and Reynolds number (Re) for the three cylinders (C1, C2, C3). At low Re values, the effects of the power-law index n and Richardson number Ri on Nu are minimal due to the low particle velocity, which results in reduced heat transfer rates. However, as Re increases, the influence of n and Ri becomes more significant. As expected, Nu increases with higher Re and Ri values. Notably, Nu also increases as the fluid behavior transitions from shear-thinning (n=0.6) to shear-thickening (n=1.6). For higher n, the shear-thickening nature of the fluid develops thicker and more stable boundary layers around the heated cylinders. These stable boundary layers enhance heat transfer, particularly in scenarios where buoyancy effects are prominent (as Ri increases). The triangular cavity geometry and the arrangement of the cylinders create recirculation zones that are influenced by fluid viscosity. Shear-thickening fluids are better at sustaining these recirculation flows, leading to improved heat transfer efficiency. For each cylinder, significant variations are observed with respect to Ri, Re, and n. The lower cylinder (C3) consistently demonstrates the highest Nu across all cases. This can be attributed to:

- The thermal buoyancy forces generating strong upward convection within the triangular cavity. These convective currents transport cooler fluid from the lower regions of the cavity directly to the surface of C3, thereby enhancing heat transfer.
- The bottom region of the cavity, near C3, forming focused recirculation zones due to the convergence of flow patterns at the triangular cavity's apex. This results in increased fluid mixing and improved heat removal.
- The triangular geometry of the cavity narrowing and accelerating the flow as it approaches the bottom. This leads to higher fluid velocities around C3, which elevate the convective heat transfer coefficient and improve cooling efficiency.

- The proximity of C3 to the cold sidewalls of the triangular cavity, resulting in a steeper local temperature gradient between the hot cylinder surface and the surrounding cooler fluid. In comparison, C1 and C2 are located higher in the cavity, where the flow has already absorbed heat from interactions with the cavity walls and other cylinders, leading to weaker temperature gradients and reduced cooling performance.

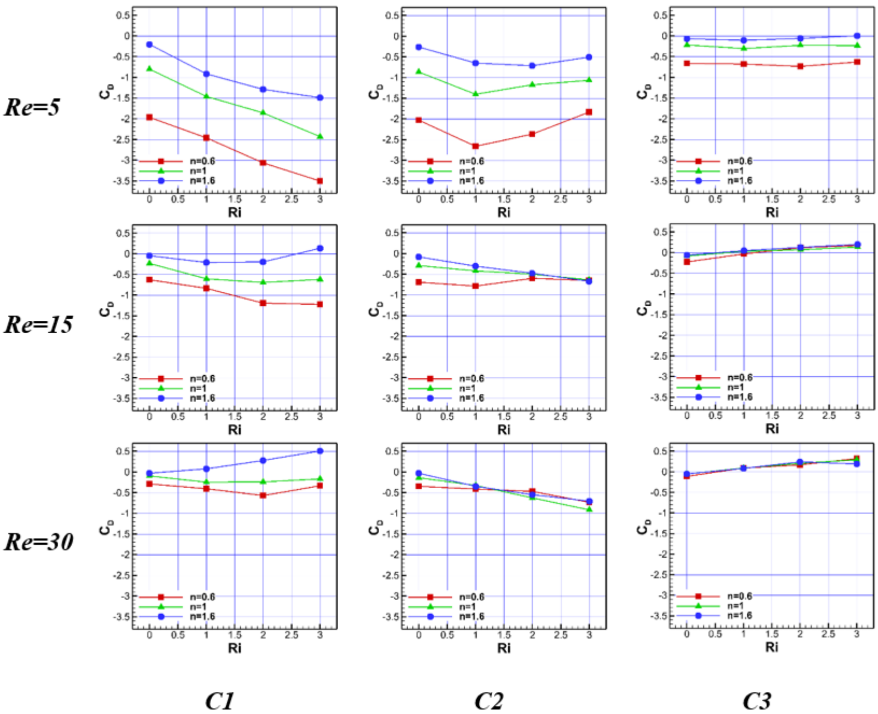

Fig. 11. Values of C_D versus Ri, n, and Re for each cylinder.

Figure 11 presents the variation of the drag coefficient (C_D) as a function of the Richardson number (Ri), power-law index (n), and Reynolds number (Re) for the three cylinders (C1, C2 and C3). The drag coefficient (C_D) can take on positive or negative values, positive C_D indicates that the drag force acts in the positive direction, while negative C_D signifies that the drag force acts in the negative direction.

At low Reynolds numbers (Re=5), the absolute magnitude of C_D is higher compared to higher Re values. This is because at lower Re, viscous forces dominate, causing greater resistance against the cylinders. As Re increases, the absolute magnitude of C_D decreases due to the increased influence of inertial forces over viscous forces. This trend is consistent across all cylinders and power-law indices. The behavior of C_D also changes with the power-law index (n). For shear-thinning fluids (n=0.6), C_D has higher magnitudes (both positive and negative) compared to shear-thickening fluids (n=1.6). This is because shear-thinning fluids experience reduced viscosity near the cylinders, leading to higher drag forces.

The drag coefficient (C_D) of the top-left cylinder (C1) is predominantly negative across all cases, indicating that the drag force acts in the negative direction. The absolute magnitude of C_D increases slightly with increasing Richardson number (Ri), which can be attributed to enhanced buoyancy forces amplifying viscous effects on the upper cylinder. For the top-right cylinder (C2),

C_D also remains negative, but has slightly lower magnitudes compared to C1. This occurs because C2 is more exposed to the interaction between the upward buoyancy-driven flow and recirculation zones, leading to reduced drag forces. The bottom cylinder (C3) exhibits the lowest C_D values among all cases and transitions from negative to positive at higher Ri values, particularly for larger power-law indices (n) and Reynolds numbers (Re). This transition indicates a shift in flow dynamics around the lower cylinder, where buoyancy becomes the dominant force, causing the drag force to align in the positive direction.

5. Conclusion

This study investigated mixed convection heat transfer and flow behavior of power-law fluids in a lid-driven triangular cavity containing three heated horizontal finned cylinders. Numerical simulations were conducted using the finite volume method, with the fluid's rheological behavior modeled via Ostwald's law. The effects of Reynolds number (Re), Richardson number (Ri), and power-law index (n) on heat transfer, flow structure, and drag coefficients were analyzed in detail. The analysis of the numerical results suggests the following conclusions:

Heat transfer is enhanced with increasing Re, Ri, and n, with the bottom cylinder (C3) exhibiting the highest Nusselt number (Nu) due to strong buoyancy-driven convection, recirculation zones, and steep temperature gradients near the cold sidewalls.

Shear-thinning fluids (n=0.6) facilitate particle movement and exhibit higher drag coefficients (C_D), while shear-thickening fluids (n=1.6) stabilize the flow and enhance boundary layer formation, leading to improved heat transfer efficiency.

The drag force direction on the bottom cylinder (C3) transitions from negative to positive at higher Ri, indicating a shift in flow dynamics driven by buoyancy forces.

The drag coefficient (C_D) decreases with Re as inertial forces dominate at higher lid velocities.

Mixed convection (Ri≠0) generates distinct counter-rotating vortices, which grow and merge as Ri and n increase.

Overall, this study provides critical insights into optimizing heat transfer and flow control in non-Newtonian fluid systems. The findings have potential applications in industries such as energy systems, thermal management, and polymer processing, where efficient heat transfer and drag reduction are crucial. Future research could explore transient effects, three-dimensional configurations, or the influence of magnetic fields to further expand the scope of this work.

References

Aboud, E. D., Rashid, H. K., Jassim, H. M., Ahmed, S. Y., Khafaji, S. O. W., Hamzah, H. K., & Ali, F. H. (2020). MHD effect on mixed convection of annulus circular enclosure filled with Non-Newtonian nanofluid. Heliyon, 6(4).

Al-Rashed A, Kalidasan K, Kolsi L, Velkennedy R, Aydi A, Husseinh A, Malekshahi E (2018). Mixed Convection and Entropy Generation in a Nanofluid filled Cubical Open Cavity with a Central Isothermal Block, International Journal of Mechanical Sciences, 135, 362-375.

Barnoon P, Toghraie D, Dehkordi R, Abed H (2019). MHD mixed convection and entropy generation in a lid-driven cavity with rotating cylinders filled by a nanofluid using two phase mixture model, Journal of Magnetism and Magnetic Materials, 483, 224–248.

Bilal S, Khan N, Fatima I, Riaz A, Ansari G, Alhazmi S, Tag El-Din E (2022). Mixed convective heat transfer in a power-law fluid in a square enclosure: Higher order finite element solutions, Frontiers in Physics, 10, 1079641.

Bilal S, Khan N, Riaz A, Alyami M, Tag El-Din E (2022). Measure and evaluate the hydrothermal flow of a Newtonian fluid in homogeneous permeable media equipped with a fin: A numerical approach, Frontiers in Physics, 10, 1032437.

Çolak E, Ekici O, Oztop H (2021). Mixed convection in a lid-driven cavity with partially heated porous block, International Communications in Heat and Mass Transfer, 126, 105450.

Gangawane K, Gupta S (2018). Mixed convection characteristics in rectangular enclosure containing heated elliptical block: Effect of direction of moving wall, International Journal of Thermal Sciences, 130, 100–115.

Gangawane K, Oztop H (2020a). Mixed convection in the semi-circular lid-driven cavity with heated curved wall subjugated to constant heat flux for non-Newtonian power-law fluids, International Communications in Heat and Mass Transfer, 114, 104563.

Gangawane K, Oztop H (2020b). Mixed convection in the heated semi-circular lid-driven cavity for non-Newtonian power-law fluids: Effect of presence and shape of the block, Chinese Journal of Chemical Engineering, 28, 1225–1240.

Gangawane K, Oztop H, Abu-Hamdeh N (2018). Mixed convection characteristic in a lid-driven cavity containing heated triangular block: Effect of location and size of block, International Journal of Heat and Mass Transfer, 124, 860–875.

Garmroodi M, Ahmadpour A, Talati F (2019). MHD mixed convection of nanofluids in the presence of multiple rotating cylinders in different configurations: a two-phase numerical Study, International Journal of Mechanical Sciences, 150, 247-264

Helmaoui, M., Laidoudi, H., Belbachir, A., Ayad, A., & Ghaniam, A. (2020). Forced convection heat transfer from a pair of circular cylinders confined in ventilated enclosure. Diffusion Foundations, 26, 104-111.

Hussain S, Jamal M, Geridonmez B (2021). Impact of power law fluid and magnetic field on double diffusive mixed convection in staggered porous cavity considering Dufour and Soret effects, International Communications in Heat and Mass Transfer, 121, 105075.

Hussain S, Oztop H (2021). Impact of inclined magnetic field and power law fluid on double diffusive mixed convection in lid-driven curvilinear cavity, International Communications in Heat and Mass Transfer, 127, 105549.

Khanafer K, Aithal S, Vafai K (2019). Mixed convection heat transfer in a differentially heated cavity with two rotating cylinders, International Journal of Thermal Sciences, 135, 117–132.

Kolsi L, Hussain S, Ghachem K, Jamal M, Maatki C (2022). Double Diffusive Natural Convection in a Square Cavity Filled with a Porous Media and a Power Law Fluid Separated by a Wavy Interface, Mathematics, 10, 1060.

Kuehn T, Goldstein R (1976). An experimental and theoretical study of natural convection in the annulus between horizontal concentric cylinders, J Fluid Mech, 74, 695-719.

Kumar S, Gangawane K, Oztop H (2021). A numerical study of mixed convection in a two-sided lid-driven tall cavity containing a heated triangular block for non-Newtonian power-law fluids, Heat Transfer, 10, 1–24.

Laidoudi H, Ameur H (2020). Investigation of the mixed convection of power-law fluids between two horizontal concentric cylinders: Effect of various operating conditions, Thermal Science and Engineering Progress, 20, 100731.

Lamsaadi M, Naimi M, Hasnaoui M (2005). Natural convection of non-Newtonian power law fluids in a shallow horizontal rectangular cavity uniformly heated from below, Heat Mass Transfer, 41, 239–249.

Lamsaadi M, Naimi M, Hasnaoui M, Mamou M (2006). Natural Convection in a Vertical Rectangular Cavity Filled with a Non-Newtonian Power Law Fluid and Subjected to a Horizontal Temperature Gradient, Numerical Heat Transfer, Part A, 49, 969–990.

Mahmood F, Chowdhury T, Hasan M (2024). Fluid-structure interaction induced mixed convection characteristics in a lid-driven square cavity with non-Newtonian power law fluids, International Journal of Thermofluids, 22, 100687.

Malkeson S, Alshaaili S, Chakraborty N (2023). Numerical investigation of steady state laminar natural convection of power-law fluids in side cooled trapezoidal enclosures heated from the bottom, Numerical Heat Transfer, Part A: Applications, 83, 770–789.

Manchanda M, Gangawane K (2018). Mixed convection in a two-sided lid-driven cavity containing heated triangular block for non-Newtonian power-law fluids, International Journal of Mechanical Sciences, 144, 235-248.

Matin MH, Khan WA (2013). Laminar natural convection of non-Newtonian power-law fluids between concentric circular cylinders. Int Commun Heat Mass Transfer, 43, 112-121.

Matin MH, Pop I, Khanchezar S (2013). Natural convection of power-law fluid between two-square eccentric ductannuli, J Non-Newtonian Fluid Mech, 197, 11-23.

Mishra L, Baranwal A, Chhabra R (2017). Laminar forced convection in power-law fluids from two heated cylinders in a square duct, International Journal of Heat and Mass Transfer, 113, 589–612.

Mohebbi R, Delouei A, Jamali A, Izadi M, Mohamad A (2019). Pore-scale simulation of non-Newtonian power-law fluid flow and forced convection in partially porous media: Thermal lattice Boltzmann method, Physica A, 525, 642–656.

Mokeddem M, Laidoudi H (2022). Mixed convection between hot and cold cylinders in square chamber: study the direction and value of the rotational speed, acta mechanica Malaysia, 5, 01-05.

Prasad D, Chaitanya G, Raju R (2019). Double diffusive effects on mixed convection Casson fluid flow past a wavy inclined plate in presence of Darcian porous medium, Results in Engineering, 3, 100019.

Rashid U, Shahzad H, Lu D, Wang X, Majeed A (2023). Non-Newtonian MHD double diffusive natural convection flow and heat transfer in a crown enclosure, Case Studies in Thermal Engineering, 41, 102541.

Rehman M, Hafeez M, Krawczuk M (2024). Computational analysis of power-law fluids for convective heat transfer in permeable enclosures using Darcy effects, Journal of Thermal Analysis and Calorimetry, 149, 6349–6360.

Rehman N, Mahmood R, Majeed A, Khan I, Mohamed A (2024). Multigrid simulations of non-Newtonian fluid flow and heat transfer in a ventilated square cavity with mixed convection and baffles, Scientific Reports, 14, 6694.

Roy P, Chowdhury S, Raj M, Islam M, Saha S (2023). Forced, natural and mixed convection of Non-Newtonian fluid flows in a square chamber with moving lid and discrete bottom heating, Results in Engineering, 17, 100939.

Selimefendigil F, Chamkha A (2019). Magnetohydrodynamics mixed convection in a power law nanofluidefilled triangular cavity with an opening using Tiwari and Das' nanofluid model, Journal of Thermal Analysis and Calorimetry Volume 135, 419–436.

Selimefendigil F, Öztop H (2018). Mixed convection of nanofluids in a three dimensional cavity with two adiabatic inner rotating cylinders, International Journal of Heat and Mass Transfer, 117, 331–343.

Thohura S, Molla M, Sarker M, Paul M (2021). Study of mixed convection flow of power-law fluids in a skewed lid-driven cavity, Heat Transfer, 10, 1–30.

Vijayan A, Gangawane K (2020). Mixed convection in a tall lid-driven cavity with a triangular heat source for non-Newtonian power-law fluids, Journal of Thermal Analysis and Calorimetry, 146, 937-954.

Zhou W, Yan Y, Liu X, Chen H, Liu B (2018). Lattice Boltzmann simulation of mixed convection of nanofluid with different heat sources in a double lid-driven cavity, International Communications in Heat and Mass Transfer, 97, 39–46.